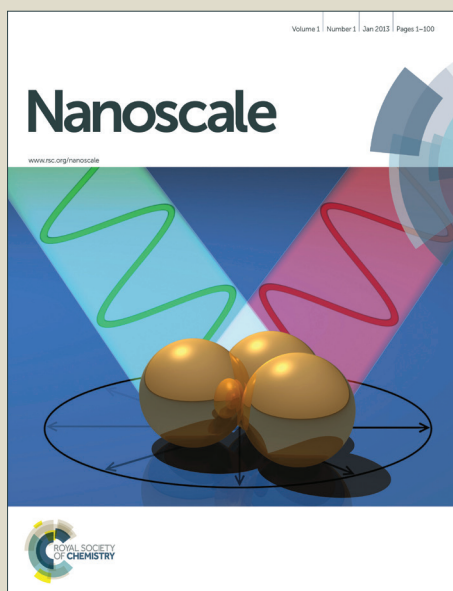


Nanoscale

Accepted Manuscript



This is an *Accepted Manuscript*, which has been through the Royal Society of Chemistry peer review process and has been accepted for publication.

Accepted Manuscripts are published online shortly after acceptance, before technical editing, formatting and proof reading. Using this free service, authors can make their results available to the community, in citable form, before we publish the edited article. We will replace this *Accepted Manuscript* with the edited and formatted *Advance Article* as soon as it is available.

You can find more information about *Accepted Manuscripts* in the [Information for Authors](#).

Please note that technical editing may introduce minor changes to the text and/or graphics, which may alter content. The journal's standard [Terms & Conditions](#) and the [Ethical guidelines](#) still apply. In no event shall the Royal Society of Chemistry be held responsible for any errors or omissions in this *Accepted Manuscript* or any consequences arising from the use of any information it contains.

ARTICLE

Stabilization of Fullerene-like Boron Cages by Transition Metal Encapsulation

Cite this: DOI: 10.1039/x0xx00000x

Jian Lv,^a Yanchao Wang,^b Lijun Zhang,^{*c} Haiqing Lin,^a Jijun Zhao^{*ad} and Yanming Ma^{*ab}

Received 00th January 2012,

Accepted 00th January 2012

DOI: 10.1039/x0xx00000x

www.rsc.org/

Stabilization of fullerene-like boron (B) cages in the free-standing form has been long sought after, but a challenging problem. Over a decade of efforts have confirmed the planar or quasi-planar polymorphs being energetically favored ground states over a wide range of small and medium-sized B clusters. Until recently, the breakthroughs represented by Nat. Chem. 6, 727 (2014) established that the transition from planar/quasi-planar to cage-like B_n clusters occurs around n ~ 38-40, paving the way for understanding intriguing chemistry of B-fullerene. We herein demonstrate that the transition demarcation n can be significantly reduced with the help of transition metal encapsulation. We explore via extensive first-principles swarm-intelligence based structure searches the free energy landscapes of B₂₄ clusters doped by a series of transition metals, and find the low-lying energy regime is generally dominated by cage-like isomers. This is in sharp contrast to that of bare B₂₄ clusters where the quasi-planar and rather irregular polyhedrons are prevalent. Most strikingly, a highly symmetric B cage in the D_{3h} symmetry is discovered under the case of Mo/W encapsulation. The endohedral D_{3h} cage exhibits robust thermodynamic, dynamical and chemical stabilities, which can be rationalized in terms of their unique electronic structure of 18-electron closed-shell configuration. Our results indicate transition metal encapsulation is a feasible route to stabilize medium-sized B cages, offering a useful roadmap for the discovery of more B fullerene analogue as building blocks of nanomaterials.

Introduction

The search for zero-dimensional fullerene-like clusters formed by elements other than carbon has been a long-standing objective¹ for expanding the inventory of available building blocks for nanoscale materials and devices. Along this direction, significant efforts have been devoted to boron (B)²⁻¹⁸ that sits next to carbon in the periodic table with only one electron deficient. Its preference of forming multiple-center chemical bonds makes it promisingly the next element after carbon capable of stabilizing a variety of low-dimensional allotropes. However, though the B cage-based motifs such as B₁₂ icosahedron are prevalent in bulk polymorphs,^{19,20} it turns out that stabilization of B fullerene analogue in the free-standing form is quite challenging. This predominantly originates from the geometrical frustration caused by the competition among a large number of isomers that are close in energy on the glass-like potential energy landscape of B clusters.²¹ In particular, for the large-sized clusters, an intriguing B₈₀ fullerene-like cage isoelectronic to C₆₀ has been theoretically proposed,² but was subsequently ruled out because of its energetic instability with respect to the core-shell type structures,²¹⁻²³ which have been

established as the ground states of large clusters of more than ~68 B atoms.²⁴ In the small and medium-sized region, it has been confirmed by gas-phase photoelectron spectroscopy and first-principle total energy calculations that the planar or quasi-planar polymorphs dominate over a wide range of sizes for B_n clusters with selected n up to 36, and there appears a tendency of deviation from the planar morphology with increasing n.²⁵⁻³⁸ It was not until quite recently that the energetically stable B fullerene analogue has been predicted in B₃₈ via a first-principle structure search study by some of us¹⁴ and discovered in B₄₀ via a photoelectron spectroscopy experiment by Zhai et al.¹⁵ The B₃₉ cage with the axially chiral feature is subsequently identified by Chen et al.³⁹ These results indicate that the transition from the planar/quasi-planar to cage-like B_n clusters occurs around a transition demarcation n ~ 38-40, promisingly paving the road for the discovery of more B-based fullerene analogues.^{40,41}

Metal encapsulation is known as an effective approach to modify chemical bondings and occupancy of energy levels of clusters, thus changing their thermodynamical and physical properties. A series of typical cage-like clusters, such as metallofullerenes⁴² and endohedrally doped silicon

fullerenes,⁴³⁻⁴⁸ have been discovered along this line. By considering the effect of metal doping in remedying the electron deficiency of B and the complex chemistry of metal-B compounds, it is reasonable to expect that the profile of potential energy landscape of B clusters will be changed significantly when some metal atom is accommodated. This may accompany with the stabilization of unstable/metastable phases of pure B clusters and emergence of new types of stable structures. In fact, the roles of metal incorporation in stabilizing new-type B clusters have been manifested in the small-size region of planar geometry, where transition-metal atoms are used to construct the sandwich-type complex (i.e. two planar B sheets connected by one metal atom)^{25,49-55} and borometallic molecular wheels (i.e. wheel morphology formed by B around the centered metal atom).⁵⁶⁻⁶⁰ Metal (or metal cluster) encapsulation has also been suggested as a possible synthesis pathway to stabilize the large-sized unstable B₈₀ fullerene analogue.^{7,61,62}

We herein probe the possibility of stabilizing B cages in the medium-sized region with single transition-metal encapsulation. Our preliminary calculations indicate that the cavities of relatively large clusters, e.g. B₃₈₋₄₀, are too big for accommodating one transition-metal atom (the metal atom is located off-centered, or anchored around surface), leading to irregular/non cage-like structures. Thus the smaller 24-atom B cluster, which has been experimentally confirmed to possess a quasi-planar structure in its anionic state,³⁸ is chosen as the target for metal encapsulation. By using first-principle energetic calculations guided by an in-house developed swarm-intelligence structure search approach,⁶³⁻⁶⁷ we have systematically investigated the potential energy landscapes of various transition-metal-doped MB₂₄ clusters (M = Ti, Zr, Hf, Cr, Mo, W, Fe, Ru and Os). The results indicate that the low-lying energy landscapes of MB₂₄ are generally dominated by cage-like structures. This is completely distinct from that of pure B₂₄ where the quasi-planar and rather irregular polyhedrons are more energetically favorable. Furthermore, for the case of Mo and W encapsulation, we find a highly symmetric B₂₄ cages (in the point group of D_{3h}) being stabilized due to their unique electronic structure with a closed 18-electron shell. Our results indicate that the transition point from quasi-planar to cage-like structures of B_n clusters can be reduced from n ~ 38-40 to n ~ 24 with suitable transition-metal encapsulation.

Computational methods

The structure search is based on globally minimizing potential energy surfaces evaluated by ab initio density functional theory (DFT) calculations, through a generalized version of particle swarm optimization algorithm specific for cluster structure prediction⁶⁴ implemented in the Crystal structure AnaLYsis by Particle Swarm Optimization (CALYPSO) code.⁶³⁻⁶⁷ Several techniques are included in the algorithm to improve the search efficiency, e.g. point group symmetries are used to generate candidate structures to avoid the appearance of liquid-like (or disordered) clusters, and bond characterization matrix technique is introduced to eliminate similar structures, etc.⁶⁴ Its validity in cluster structure prediction has been demonstrated by its successfully identifying the ground-state structures for a series of cluster systems.^{14,68,69} The underlying energetic

calculation and local structure optimization were performed at the DFT level using the Perdew–Burke–Ernzerhof generalized gradient functional with a predefined amount of exact exchange (hybrid PBE0)⁷⁰ through the Gaussian 09 Package.⁷¹ Since thousands of sampled structures are subject to evaluation during the structure search, an economic basis set, i.e. the 3-21 basis set for B and Stuttgart basis set⁷²⁻⁷⁶ for the transition metals, is chosen and only singlet spin state is considered. These settings are enough for evaluating the relative energy of sampled structures. After the structure search, the accurate basis set of 6-311G* for B with full consideration of multiple spin states is used for refined structure optimization and vibrational frequency calculation for the isomers with low-lying energy. The suitability of the PBE0 functional in reliably describing the energy difference among the isomers of medium-sized boron clusters has been benchmarked in Ref. 24 by comparison with the higher-level CCSD(T) results. The molecular dynamics simulations and formation energy calculations are carried out using the plane wave basis set, projected augmented wave potentials,^{77,78} and PBE exchange-correlation functional⁷⁹ through the Vienna ab initio simulation package.⁸⁰ The cutoff energy of 500 eV for wave-function expansion and the Monkhorst-Pack k-mesh sampling (Γ point for B clusters, 20x20x20 for transition metals and 12x12x12 for α-B) are chosen to ensure the total energy converged better than 1 meV/atom. For such calculations with periodic boundary condition, a vacuum region of 12 Å was used to isolate finite clusters and avoid their interactions with adjacent periodic images.

Results and discussion

Potential energy landscape of MB₂₄ clusters: dominated by cage-like structures.

We start with a direct comparison between the general potential energy landscapes of bare B₂₄ and MB₂₄ clusters. For each case, our structure search probes more than 2000 points on the potential energy surface from three independent simulations with randomly generated initial structures. Fig. 1a and 1b show the energy of all the sampled structures as the function of evolution step for bare B₂₄ and W-encapsulated WB₂₄ clusters, respectively. To classify the sampled structures in terms of their morphology, a parameter δ reflecting the deviation from perfectly spherical cage is defined as,

$$\delta = \sqrt{\frac{1}{24} \sum_{n=1}^{24} (r_i - r_0)^2},$$

where r_0 is the averaged distance from all B atoms to their mass center and r_i is the distance from the i -th B atom to the mass center. The δ values for all the structures are indicated in Fig. 1 by color-coding. Visual inspection of the structures indicates that the case with $\delta < 0.5$ Å can be classified as cage-like structure, whereas $\delta > 1.0$ Å represents quite irregular polyhedron or quasi-planar geometry. We can see that for the bare B₂₄ clusters (Fig. 1a), the low-lying energy region of potential energy surface is dominated by irregularly polyhedral and quasi-planar structures, and the complicated competition among them spans the whole range of evolution steps (up to a

large value of 45). This is consistent with the previous report of the quasi-planar and tubular structures being stable isomers.^{38,81–83} Turning to the W-encapsulated case (Fig. 1b), the potential energy landscape can be generally divided into the low-lying part occupied by the cage-like structures and the high-lying part composed of irregularly polyhedral structures. From the 2nd evolution step, the cage-like structure has become the ground-state isomer, and with increasing step, more cage-like structures emerge in the low-lying energy region, indicating their robustly energetic favorability. The lowest-energy ground-state isomers for nine transition-metal-doped MB₂₄ clusters (M = Ti, Zr, Hf, Cr, Mo, W, Fe, Ru and Os) are shown in Fig. 2 (the Cartesian coordinates of the lowest-energy structures are given in Tables SI-SIX in the ESI† and more low-lying energy isomers for each cluster are given in Figs. S1–S9 in the ESI†). As seen, the low-lying energy isomers of all the nine cases take cage-like morphologies.

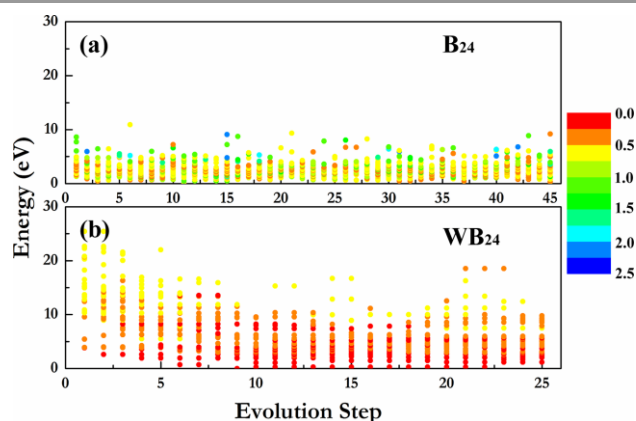


Fig. 1. Energetics of all the sampled structures during the structure search as the function of evolution step for (a) bare B₂₄ and (b) WB₂₄ clusters, respectively. Color-coding of each structure point denotes the deviation of its morphology from perfectly spherical cage, which is characterized by a defined parameter δ (see the main text). The smaller δ (more red) corresponds to regular cage-like structure, whereas the larger δ (more blue) represents irregular or quasi-planar structure.

Meanwhile, from Fig. 1a we note that the energy span width of B₂₄ is rather small (~10 eV), which reveals the existence of a large number of different structures with similar energetics, in accord with the report of the glass-like energy landscape of B clusters by Goedecker and coauthors.²¹ Differently the energy span width of WB₂₄ (Fig. 1b) is more than 20 eV, two times larger than that of B₂₄. This implies that the glass-like energy landscape of B₂₄ is changed dramatically after transition-metal encapsulated, where a global basin-like profile filled with cage-like structures dominates.

Highly symmetric B₂₄ cages stabilized by Mo/W encapsulation.

Walking through the ground-state structures of all the MB₂₄ (Fig. 2), we find that for M = Ti, Zr, Hf, Cr, Fe, Ru and Os, although the ground-state structure takes the cage-like geometry, the abnormality is substantially large (with $\delta = 0.1$ – 0.43 Å), accompanying with a low symmetry of C_s or C₁. In most of cases (e.g. M = Ti, Hf, Fe, Ru and Os), there exist

several isomers with nearly degenerate energies with respect to the ground state. For such low-symmetry clusters, there is a higher possibility of existing low transition barriers among the ground-state and other higher-energy metastable structures.^{84,85} Thus their ground-state structures are usually quite chemically active, difficult to be stabilized under normal kinetic control. However, this is not the case for M = Mo and W: a highly symmetric B₂₄ cage (with $\delta = 0.05$ Å) in the point group of D_{3h} becomes the ground-state structure. The D_{3h}-MoB₂₄ and D_{3h}-WB₂₄ cages can be viewed as three bent B₆ clusters²⁵ parallel to the principal axis jointed by six boron atoms, mainly composed of two hexagons on the bottom and top, three hexagons and three squares alternatively surrounding the waist.

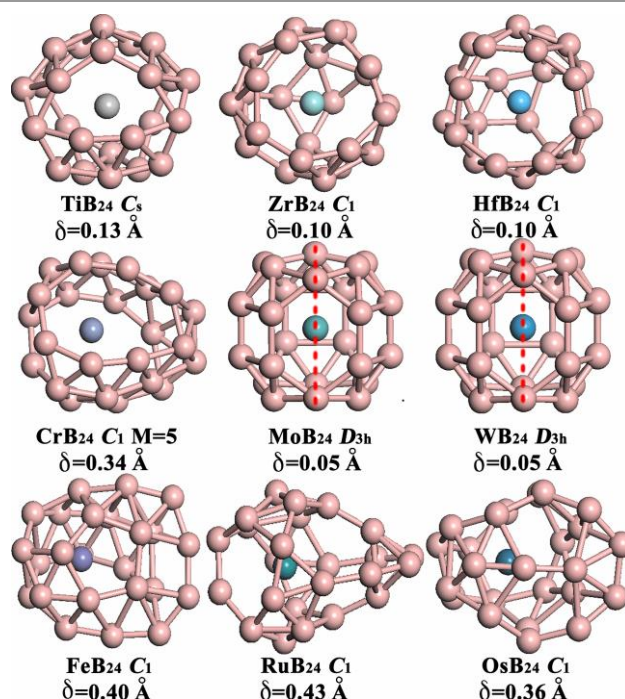


Fig. 2. The lowest-energy ground-state isomers of MB₂₄ (M = Ti, Zr, Hf, Cr, Mo, W, Fe, Ru and Os) clusters derived from the global minimum structure search. For each system, the point-group symmetry and the δ value in Fig. 1 (reflecting the deviation of the morphology from spherical cage) are indicated. Spin multiplicity is given for the isomer taking non-singlet spin state as the ground state.

We take the WB₂₄ case as a representative to show robustly energetic stability of the high-symmetry D_{3h} cage. Fig. 3 shows selected low-lying energy structures (I–VII) found by the structure search, with their symmetry and energy relative to the ground-state D_{3h} cage (I), and their Cartesian coordinates are given in Tables SX–SXVI in the ESI†. The lowest metastable isomer II is less stable than the D_{3h} cage by a large amount of energy (0.29 eV). Its structure is similar to the D_{3h} cage, but in a D_{3d} symmetry, consisting of six pentagons surrounding the waist. Despite of their structural similarity, a transition state optimization using the synchronous Transit-Guided quasi-Newton method⁸⁶ reveals a rather high transition barrier of 0.53 eV between them with only one imaginary frequency at 2631 cm⁻¹. There emerges another metastable cage in the higher symmetry of D_{2h} (isomer V), but 0.77 eV higher in

energy than the D_{3h} cage. For the isomer VI and VII with the much higher energies, the irregularity of cages increases dramatically with the appearance of big holes on the surfaces. This tendency is consistent with Fig. 1b, where irregularly polyhedral structures dominate the high-lying energy region. The preference of W atom staying at the central position is examined by moving W out of the D_{3h} cage (in two different ways); the resulted structures (isomer VIII and IX) show remarkable instability (with respect to the D_{3h} cage) evidenced by a large energy difference of 4.48 and 4.83 eV, respectively. Additionally, we have constructed more isomers based on the known structural motifs of bare B clusters, for instance, by placing W atom at the center of double-ring and three-ring tubular clusters⁸³ (isomer X and XI), and the sandwich-type structure through resembling quasi-planar B_{12} cluster²⁷ (isomer XII); all these structures show much higher energies (>2.5 eV) than the D_{3h} cage.

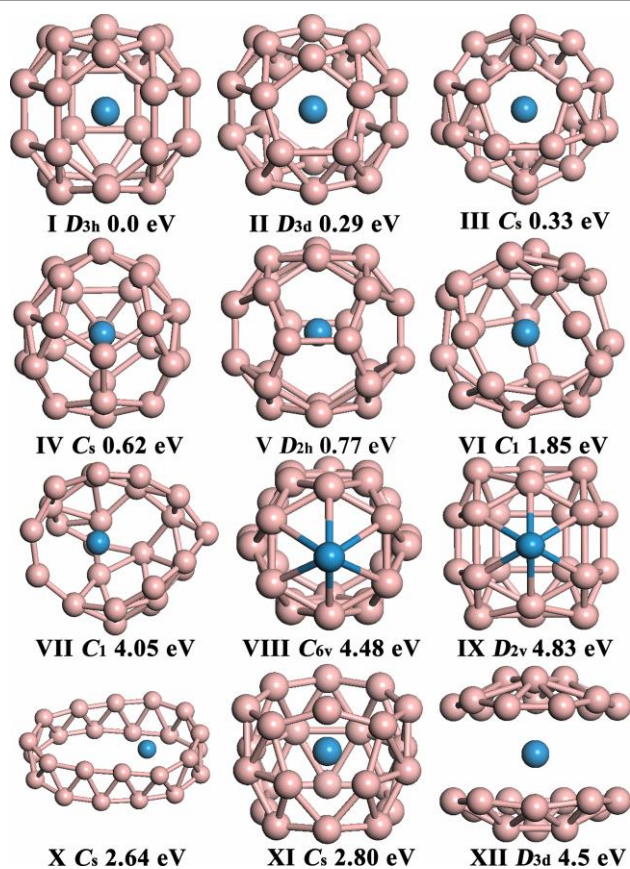


Fig. 3. Low-lying energy structures of WB_{24} from the structure search (I-VII), as well as specially designed structures to verify the stability of the ground-state isomer I (see text, VIII-XII). For each structure, the point-group symmetry and the energy relative to isomer I are indicated. The zero-point energy corrections are taken into account by using harmonic vibrational frequencies.

Formation energy and dynamical stability of D_{3h} - MoB_{24} and D_{3h} - WB_{24} cages.

We then calculate formation energies (E_f , defined as the energy difference per atom between cluster and corresponding bulk counterparts) of D_{3h} - MoB_{24} and D_{3h} - WB_{24} cages and compare

them with that of bare B_{24} clusters. By using the ground-state planar structure of anionic specie³⁸ and the quasi-planar double-ring tubular structure of neutral specie,⁸¹⁻⁸³ the calculated E_f of bare B_{24} is 0.85 and 0.79 eV/atom, respectively. For D_{3h} - MoB_{24} and D_{3h} - WB_{24} , the E_f values are 0.72 and 0.74 eV/atom, which are about 50 meV/atom lower than that of the double-ring tubular B_{24} and 100 meV/atom lower than that of the planar B_{24} . In spite of the still positive E_f values, which are common for the metastable polymorphs of nanoscale clusters, the reduced magnitudes imply enhanced thermodynamic stability of endohedral cages.

To evaluate dynamical stabilities, vibrational frequencies are calculated. For both D_{3h} - MoB_{24} and D_{3h} - WB_{24} , no imaginary frequency is observed and the lowest frequencies sufficiently above the stability criterion of 100 cm^{-1} suggested by Hoffmann *et al.*⁸⁷ Moreover, high-temperature structural stability (of D_{3h} - WB_{24}) is examined by constant-temperature molecular dynamics simulation at 800 K. No sign of structural deformation is observed over 20000 steps with a time step size of 0.5 fs.

For the highly symmetric D_{3h} - MoB_{24} and D_{3h} - WB_{24} cages, the calculated natural atomic charges (*i.e.* nuclear charge minus summed populations of the natural atomic orbitals on the atom) are -2.75 and -2.59 e for Mo and W, and small positive values (about +0.2 e) for most of B. This moderate charge transfer from B cages to metal atoms is consistent with the fact of the slightly larger electronegativity of Mo and W (2.16 and 2.36 by Pauling scale) than that of B (2.04). Meanwhile, no electron localization can be found between metal atoms and B on the cages in the electron localization function plots as shown in Fig. S16 in the ESI†. These indicate that the bondings between Mo/W and B are predominantly ionic.

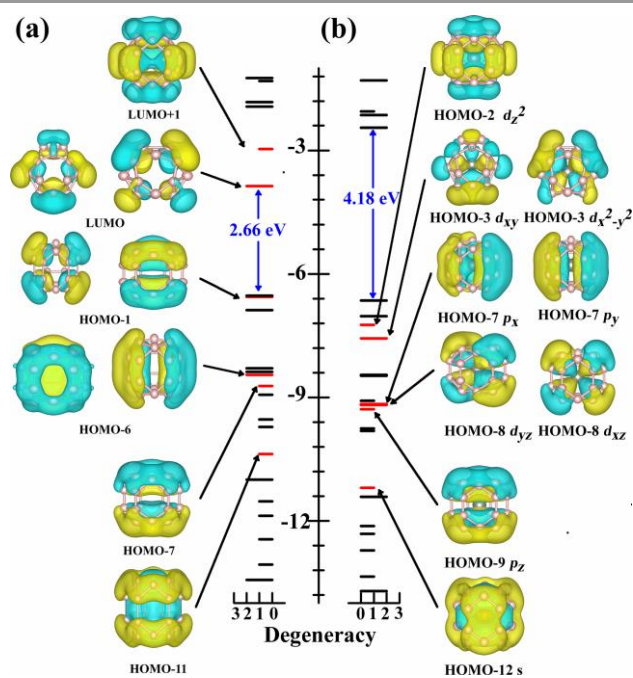


Fig. 4. Eigenvalue spectra vs electronic state degeneracy of (a) bare D_{3h} - B_{24} cage and (b) D_{3h} - WB_{24} . For each case, the HOMO-LUMO gap is indicated (in blue). The

π -orbitals (red lines) for (a) and the orbitals involving 18-electron closed-shell configuration (see text) in (b) are shown.

Origin of the endohedral D_{3h} cage being stabilized: formation of 18-electron closed-shell configuration.

Further molecular-orbital analysis of electronic structure indicates that the stability of the D_{3h} cage with Mo/W encapsulation can be rationalized by the mutual interaction between the π -electrons of B cages and the valence electron states of Mo/W. Fig. 4 shows the side-by-side comparison of eigenvalue spectra for the D_{3h} cage without (a, bare D_{3h} - B_{24}) and with (b) W encapsulation. One clearly notes that the HOMO-LUMO gap (E_{H-L}) is significantly increased from 2.66 eV of bare D_{3h} - B_{24} (2.19 eV of the planar and double-ring tubular B_{24} clusters) to 4.18 eV of D_{3h} - WB_{24} (4.21 eV of D_{3h} - MoB_{24}). This underlies strong chemical stability of the endohedral D_{3h} cages.⁸⁸ For bare D_{3h} - B_{24} (Fig. 4a), there are 6 occupied π -orbitals (HOMO-1, 6, 7, and 11) and 3 unoccupied π -orbitals (LUMO and LUMO+1). The moderate E_{H-L} is attributed to the mid-lying binding energies of the latter. Because of the out-of-surface delocalized feature of these π -orbitals, they will interact with the electronic orbitals of interior Mo/W atoms in the endohedral cages, forming hybridized orbitals. As the group-VIB element, Mo/W has 6 valence electrons, plus 12 π -electrons (from 6 occupied π -orbitals) of bare D_{3h} - B_{24} , giving totally 18 electrons to be placed into the newly formed orbitals. For the current cluster systems, which can be viewed as artificial atoms, this special electron counting number of 18 is favorable for forming a stable 18-electron closed-shell configuration. The mechanism is similar to that of the transition metal complexes, such as ferrocene $Fe(C_5H_5)_2$ ⁸⁹ and chromium hexacarbonyl $Cr(CO)_6$.⁹⁰ As depicted in Fig. 4b, in D_{3h} - WB_{24} we indeed find 9 occupied atomic-like orbitals resembling those of inert-gas elements, which are formed through the “sp d - π interaction/hybridization”,⁵⁵ i.e. HOMO-12 (s-like), HOMO-9 (p_z -like), HOMO-8 (doubly degenerate, d_{xy} -like and d_{yz} -like), HOMO-7 (p_y -like and p_x -like), HOMO-3 ($d_x^2-y^2$ -like and d_{xy} -like) and HOMO-2 (d_z^2 -like). This closed-shell electron configuration results in substantial energy gain, significantly increasing structural stability of the endohedral D_{3h} cages. The orbital hybridization and electron redistribution eliminate the 3 unoccupied π -orbitals of bare D_{3h} - B_{24} , enlarging the E_{H-L} . However, this is not the case for the isoelectronic CrB_{24} system, where the endohedral D_{3h} cage is less stable than the ground-state C_1 cage by 0.33 eV (Fig. S4 in the ESI†). This may be attributed to the smaller size of the Cr atom, which is not optimal to fit the cavity of the D_{3h} cage, thus geometry frustration becoming energetically favorable.

The responsibility of forming the 18-electron closed-shell configuration for stabilizing the endohedral D_{3h} cage is further evidenced by investigating other MB_{24} ($M = Ti, Zr, Hf, Fe, Ru$ and Os) systems with enforced electron counting number of 18. In particular, for each case we take all the low-lying energy structures of nine MB_{24} systems from the structure search and reoptimize them at the dianionic (for $M = Ti, Zr$ and Hf) or dicationic (for $M = Fe, Ru$ and Os) charge state. Corresponding

uniform compensated background charge is applied to guarantee the charge neutral condition. The resulted low-lying energy isomers are summarized in Figs. S10 – S15 in the ESI†. With the fulfilled 18-electron discipline, the D_{3h} endohedral cage becomes the lowest-energy structure for most of cases except for FeB_{24} . The violation of FeB_{24} can be understood by the even smaller atomic radius (1.32 Å) of Fe than that of Cr (1.39 Å), thus too small to be comfortably accommodated in the void of the high-symmetry D_{3h} cage.

We calculate typical satellite properties of 18-electron systems for D_{3h} - MoB_{24} and D_{3h} - WB_{24} , and compare them with those of other known 18-electron systems, such as $Fe(C_5H_5)_2$, $Cr(CO)_6$, $CrSi_{12}$ ⁴⁶ and WSi_{12} .^{45,48} As listed in Table I, the properties include the binding energy (E_b , the energy difference between cluster and constituent atoms), HOMO-LUMO energy gap (E_{H-L}), vertical electron affinities (VEAs, the energy difference between neutral and anionic clusters at the geometry of neutral cluster), vertical ionization potentials (VIPs, the energy difference between cationic and neutral clusters at the geometry of neutral cluster), as well as the difference between VIP and VEA (chemical hardness,^{91,92} a useful metric for estimating the stability of molecules and clusters). Taking the chemical hardness as the example, the values of D_{3h} - MoB_{24} and D_{3h} - WB_{24} are 6.80 and 6.77 eV, which are slightly lower than those of $Fe(C_5H_5)_2$ (7.24 eV) and $Cr(CO)_6$ (8.86 eV), but much larger than those of $CrSi_{12}$ (4.18 eV) and WSi_{12} (5.14 eV). Other properties follow the similar trend. These results show further evidence of the endohedral D_{3h} cages belonging to the 18-electron closed-shell family.

Table I. The binding energies (E_b), HOMO-LUMO gaps (E_{H-L}), vertical electron affinities (VEAs), vertical ionization potentials (VIPs), differences between VIP and VEA of D_{3h} - MoB_{24} and D_{3h} - WB_{24} , compared with those of typical 18-electron systems ($Fe(C_5H_5)_2$, $Cr(CO)_6$, $CrSi_{12}$ and WSi_{12}).

System	E_b (eV/atom)	E_{H-L} (eV)	VEA (eV)	VIP(eV)	VIP-VEA(eV)
$Fe(C_5H_5)_2$	-4.81	5.76	-0.21	7.03	7.24
$Cr(CO)_6$	-5.59	6.06	-0.16	8.70	8.86
$CrSi_{12}$	-3.45	3.36	3.49	7.67	4.18
WSi_{12}	-3.87	3.09	2.65	7.79	5.14
D_{3h} - MoB_{24}	-5.37	4.21	1.20	8.00	6.80
D_{3h} - WB_{24}	-5.43	4.18	1.26	8.03	6.77

The mechanism of the current medium-size endohedral B_{24} cages being stabilized is different from the case of the endohedral fullerenes⁴². In endohedral fullerenes, since the carbon cages are inherently stable, the central problem is to find the suitable metal atoms that are stable in the center of the cage. The doped metal atoms donate charge to the cage, and are bound to the cage wall through the Coulomb interactions.⁹³ Here the bare B_{24} cages are chemically unstable against the quasi-planar isomers, and the incorporation of transition metal atoms is the prerequisite to stabilize the cages. For the case of Mo/W encapsulation, the charge transfer occurs reversely from B cages to metal atoms as mentioned and the formation of 18-

electron closed-shell configuration ensures the strong chemical stability of the highly symmetric D_{3h} cage. This mechanism is also distinct from that of the reported larger-size endohedral MB_{40} ($M = Ca, Sr, Sc, Y, La$) cages,^{40,41} which is essentially similar to the case of endohedral fullerenes.

Conclusions

In summary, with the aim of stabilizing fullerene-like B cages in medium-sized clusters, we performed an unbiased first-principle structure search study for the B_{24} clusters doped by a series of transition metals including Ti, Zr, Hf, Cr, Mo, W, Fe, Ru and Os. We found the free energy landscapes of B_{24} clusters are qualitatively changed after transition metal encapsulation, where the cage-like rather than originally quasi-planar polymorphs emerge as energetically favorable isomers. While most of stable endohedral cages possess low symmetries, a high-symmetry D_{3h} cage is stabilized by Mo/W encapsulation. This endohedral D_{3h} cage exhibits high chemical stability as indicated by its large binding energy, high HOMO-LUMO gap and chemical hardness. All these properties can be rationalized in terms of its unique electronic structure of 18-electron closed-shell configuration. The high transition barrier between it and other competitive isomers associated with its high symmetry is favorable for kinetic stability with respect to variations of external conditions. Experimental attempt to synthesize this novel endohedral D_{3h} cage is called for. It should be pointed out that the currently uncovered endohedral B_{24} cage exists through a coincidence of electronic and geometrical factors. The 18-electron rule, which is responsible for the high chemical stability of high-symmetry endohedral D_{3h} cage, can only be satisfied if the cluster size and the valence electrons of transition metals match the optimal bondings between the cage and metal atoms. With reasonable choices of transition metal atom and appropriate number of B atoms, other sized B cages are also likely to be stabilized. The present results are thus promisingly to open a door for the discovery of more endohedral B fullerene analogues.

Acknowledgements

The authors acknowledge funding support from the National Natural Science Foundation of China (under Grants No. 11274136 and No. 11404128), the Postdoctoral Science Foundation of China (No. 2014M550596 and 2014M551181), 2012 Changjiang Scholar of Ministry of Education and the China 973 Program under Grant No. 2011CB808204. L.Z. acknowledges funding support from the Recruitment Program of Global Experts (the Thousand Young Talents Plan). Part of the calculations was performed in the high performance computing center of Jilin University.

Notes and references

^a Beijing Computational Science Research Center, Beijing 100084, China

^b State Key Laboratory of Superhard Materials, Jilin University, Changchun 130012, China. E-mail: mym@calypso.cn

^c College of Materials Science and Engineering and Key Laboratory of Automobile Materials of MOE, Jilin University, Changchun 130012, China. E-mail: lijun_zhang@jlu.edu.cn

^d Key Laboratory of Materials Modification by Laser, Ion and Electron Beams (Dalian University of Technology), Ministry of Education, Dalian 116024, China. E-mail: zhaoji@dlut.edu.cn

† Electronic Supplementary Information (ESI) available: See DOI: 10.1039/b000000x/

1. J. Zhao, L. Ma, D. Tian and R. Xie, *J. Comput. Theor. Nanosci.*, 2008, **5**, 7.
2. N. Gonzalez Szwacki, A. Sadrzadeh, and B. Yakobson, *Phys. Rev. Lett.*, 2007, **98**, 166804.
3. L. Cheng, *J. Chem. Phys.*, 2012, **136**, 104301.
4. W. Hayami and S. Otani, *J. Phys. Chem. A*, 2011, **115**, 8204–8207.
5. R. R. Zope and T. Baruah, *Chem. Phys. Lett.*, 2011, **501**, 193–196.
6. J. T. Muya, G. Gopakumar, M. T. Nguyen, and A. Ceulemans, *Phys. Chem. Chem. Phys.*, 2011, **13**, 7524–7533.
7. P. Pochet, L. Genovese, S. De, S. Goedecker, and D. Caliste, *Phys. Rev. B*, 2011, **83**, 081403.
8. K. D. Quarles, C. B. Kah, and R. N. Gunasinghe, *J. Chem. Theory Comput.*, 2011, **7**, 2017–2020.
9. L. Wang, J. Zhao, F. Li, and Z. Chen, *Chem. Phys. Lett.*, 2010, **501**, 16–19.
10. X.-Q. Wang, *Phys. Rev. B*, 2010, **82**, 153409.
11. X.-L. Sheng, Q.-B. Yan, Q.-R. Zheng, and G. Su, *Phys. Chem. Chem. Phys.*, 2009, **11**, 9696–9702.
12. Q.-B. Yan, X.-L. Sheng, Q.-R. Zheng, L.-Z. Zhang, and G. Su, *Phys. Rev. B*, 2008, **78**, 201401.
13. D. Prasad and E. Jemmis, *Phys. Rev. Lett.*, 2008, **100**, 165504.
14. J. Lv, Y. Wang, L. Zhu, and Y. Ma, *Nanoscale*, 2014, **6**, 11692–11696.
15. H.-J. Zhai, Y.-F. Zhao, W.-L. Li, Q. Chen, H. Bai, H.-S. Hu, Z. A. Piazza, W.-J. Tian, H.-G. Lu, Y.-B. Wu, Y.-W. Mu, G.-F. Wei, Z.-P. Liu, J. Li, S.-D. Li, and L. S. Wang, *Nat. Chem.*, 2014, **6**, 727.
16. J. T. Muya, E. Lijnen, M. T. Nguyen, and A. Ceulemans, *Chem. Phys. Chem.*, 2013, **14**, 346–363.
17. H. Lu and S.-D. Li, *J. Chem. Phys.*, 2013, **139**, 224307.
18. S. Polad and M. Ozay, *Phys. Chem. Chem. Phys.*, 2013, **15**, 19819.
19. B. Albert and H. Hillebrecht, *Angew. Chem. Int. Ed.*, 2009, **48**, 8640–8668.
20. J. Donohue, *The Structures of the Elements*, John Wiley & Sons Incorporated, 1974.
21. S. De, A. Willand, M. Amsler, P. Pochet, L. Genovese, and S. Goedecker, *Phys. Rev. Lett.* 2011, **106**, 225502.
22. J. Zhao, L. Wang, F. Li, and Z. Chen, *J. Phys. Chem. A*, 2010, **114**, 9969–9972.
23. H. Li, N. Shao, B. Shang, L.-F. Yuan, J. Yang, and X. C. Zeng, *Chem. Commun.*, 2010, **46**, 3878–3880.
24. F. Li, P. Jin, D. Jiang, L. Wang, and S. B. Zhang, *J. Chem. Phys.*, 2012, **136**, 047302.
25. A. N. Alexandrova, A. I. Boldyrev, H.-J. Zhai, and L. S. Wang, *J. Chem. Phys.*, 2005, **122**, 054313.
26. H.-J. Zhai, A. N. Alexandrova, K. A. Birch, A. I. Boldyrev, and L. S. Wang, *Angew. Chem. Int. Ed.*, 2003, **42**, 6004–6008.
27. H.-J. Zhai, B. Kiran, J. Li, and L. S. Wang, *Nat. Mater.*, 2003, **2**, 827–833.
28. A. P. Sergeeva, D. Y. Zubarev, H.-J. Zhai, A. I. Boldyrev, and L. S. Wang, *J. Am. Chem. Soc.*, 2008, **130**, 7244–7246.
29. B. Kiran, S. Bulusu, H.-J. Zhai, S. Yoo, X. C. Zeng, and L. S. Wang, *Proc. Natl. Acad. Sci. U. S. A.*, 2005, **102**, 961–964.

30. W.-L. Li, Q. Chen, W.-J. Tian, H. Bai, Y.-F. Zhao, H.-S. Hu, J. Li, H.-J. Zhai, S.-D. Li, and L. S. Wang, *J. Am. Chem. Soc.*, 2014, **136**, 12257–12260.
31. W.-L. Li, Y.-F. Zhao, H.-S. Hu, J. Li, and L. S. Wang, *Angew. Chem. Int. Ed.*, 2014, **53**, 5540–5545.
32. Z. A. Piazza, H.-S. Hu, W.-L. Li, Y.-F. Zhao, J. Li, and L. S. Wang, *Nat. Commun.*, 2014, **5**, 3113.
33. A. P. Sergeeva, Z. A. Piazza, C. Romanescu, W.-L. Li, A. I. Boldyrev, and L. S. Wang, *J. Am. Chem. Soc.*, 2012, **134**, 18065–18073.
34. Z. A. Piazza, W.-L. Li, C. Romanescu, A. P. Sergeeva, L. S. Wang, and A. I. Boldyrev, *J. Chem. Phys.*, 2012, **136**, 104310.
35. C. Romanescu, D. J. Harding, A. Fielicke, and L. S. Wang, *J. Chem. Phys.*, 2012, **137**, 014317.
36. A. P. Sergeeva, B. B. Averkiev, H.-J. Zhai, A. I. Boldyrev, and L. S. Wang, *J. Chem. Phys.*, 2011, **134**, 224304.
37. Z. A. Piazza, I. A. Popov, W.-L. Li, R. Pal, X. Cheng Zeng, A. I. Boldyrev, and L. S. Wang, *J. Chem. Phys.*, 2014, **141**, 034303.
38. I. A. Popov, Z. A. Piazza, W.-L. Li, L. S. Wang, and A. I. Boldyrev, *J. Chem. Phys.*, 2013, **139**, 144307.
39. Q. Chen, W.-L. Li, Y.-F. Zhao, S.-Y. Zhang, H.-S. Hu, H. Bai, H.-R. Li, W.-J. Tian, H.-G. Lu, H.-J. Zhai, S.-D. Li, J. Li, and L. S. Wang, *ACS Nano*, 2015, **9**, 754–760.
40. P. Jin, Q. Hou, C. Tang, and Z. Chen, *Theor. Chem. Acc.*, 2015, **134**, 13–10.
41. H. Bai, Q. Chen, H.-J. Zhai, and S.-D. Li, *Angew. Chem. Int. Ed.*, 2014, **54**, 941–945.
42. Y. Chai, T. Guo, C. Jin, R. E. Haufler, Chibante, L. P. Felipe, J. Fure, L. Wang, J. M. Alford, and R. E. Smalley, *J. Phys. Chem.*, 1991, **95**, 7564–7568.
43. H. G. Xu, X. Y. Kong, X. J. Deng, and Z. G. Zhang, *J. Chem. Phys.*, 2014, **140**, 024308.
44. K. Koyasu, M. Akutsu, M. Mitsui, and A. Nakajima, *J. Am. Chem. Soc.*, 2005, **127**, 4998–4999.
45. T. Miyazaki, H. Hiura, and T. Kanayama, *Eur. Phys. J. D*, 2003, **24**, 241–244.
46. S. Khanna, B. Rao, and P. Jena, *Phys. Rev. Lett.*, 2002, **89**, 016803.
47. V. Kumar and Y. Kawazoe, 2001, *Phys. Rev. Lett.*, **87**, 045503.
48. H. Hiura, T. Miyazaki, and T. Kanayama, *Phys. Rev. Lett.*, 2001, **86**, 1733–1736.
49. L.-M. Yang, J. Wang, Y.-H. Ding, and C.-C. Sun, *J. Phys. Chem. A*, 2007, **111**, 9122–9129.
50. S.-D. Li, C.-Q. Miao, J.-C. Guo, and G.-M. Ren, *J. Comput. Chem.*, 2006, **27**, 1858–1865.
51. S.-D. Li, J.-C. Guo, C.-Q. Miao, and G.-M. Ren, *Angew. Chem. Int. Ed.*, 2005, **44**, 2158–2161.
52. A. N. Alexandrova, H.-J. Zhai, L. S. Wang, and A. I. Boldyrev, *Inorg. Chem.*, 2004, **43**, 3552–3554.
53. Q. S. Li and Q. Jin, *J. Phys. Chem. A*, 2003, **107**, 7869–7873.
54. A. N. Alexandrova, A. I. Boldyrev, H.-J. Zhai, and L. S. Wang, *Coord. Chem. Rev.*, 2006, **250**, 2811–2866.
55. Y. Yuan and L. Cheng, *J. Chem. Phys.*, 2013, **138**, 024301.
56. T. Heine and G. Merino, *Angew. Chem. Int. Ed.*, 2012, **51**, 4275–4276.
57. T. R. Galeev, C. Romanescu, W.-L. Li, L. S. Wang, and A. I. Boldyrev, *Angew. Chem. Int. Ed.*, 2012, **51**, 2101–2105.
58. W.-L. Li, C. Romanescu, T. R. Galeev, Z. A. Piazza, A. I. Boldyrev, and L. S. Wang, *J. Am. Chem. Soc.*, 2012, **134**, 165–168.
59. C. Romanescu, T. R. Galeev, A. P. Sergeeva, W.-L. Li, L. S. Wang, and A. I. Boldyrev, *J. Organomet. Chem.*, 2012, **721–722**, 148–154.
60. C. Romanescu, T. R. Galeev, W.-L. Li, A. I. Boldyrev, and L. S. Wang, *Angew. Chem. Int. Ed.*, 2011, **50**, 9334–9337.
61. P. Boulanger, M. Morinière, L. Genovese, and P. Pochet, *J. Chem. Phys.*, 2013, **138**, 184302.
62. P. Jin, C. Hao, Z. Gao, S. B. Zhang, and Z. Chen, *J. Phys. Chem. A*, 2009, **113**, 11613–11618.
63. Y. Wang, J. Lv, L. Zhu, and Y. Ma, *Comput. Phys. Commun.*, 2012, **183**, 2063–2070.
64. J. Lv, Y. Wang, L. Zhu, and Y. Ma, *J. Chem. Phys.*, 2012, **137**, 084104.
65. Y. Wang, M. Miao, J. Lv, L. Zhu, K. Yin, H. Liu, and Y. Ma, *J. Chem. Phys.*, 2012, **137**, 224108.
66. Y. Wang, J. Lv, L. Zhu, and Y. Ma, *Phys. Rev. B*, 2010, **82**, 094116.
67. S. Lu, Y. Wang, H. Liu, M.-S. Miao, and Y. Ma, *Nat. Commun.*, 2014, **5**, 1–6.
68. M. Ju, J. Lv, X.-Y. Kuang, L.-P. Ding, C. Lu, J.-J. Wang, Y.-Y. Jin, and G. Maroulis, *RSC Adv.*, 2014, **5**, 6560–6570.
69. S. F. Li, X. J. Zhao, X. S. Xu, Y. F. Gao, and Z. Zhang, *Phys. Rev. Lett.*, 2013, **111**, 115501.
70. C. Adamo and V. Barone, *J. Chem. Phys.*, 1999, **110**, 6158.
71. Frisch, M. J. et al. Gaussian 09, revision C.01; Gaussian, Inc.: Wallingford, CT, 2009.
72. M. Dolg, U. Wedig, H. Stoll, and H. Preuss, *J. Chem. Phys.*, 1987, **86**, 866.
73. M. Kaupp, P. V. R. Schleyer, H. Stoll, and H. Preuss, *J. Chem. Phys.*, 1991, **94**, 1360.
74. A. Bergner, M. Dolg, W. Küchle, H. Stoll, and H. Preuss, *Mol. Phys.*, 1993, **80**, 1431–1441.
75. M. Dolg, H. Stoll, H. Preuss, and R. M. Pitzer, *J. Phys. Chem.*, 1993, **97**, 5852–5859.
76. P. Schwerdtfeger, M. Dolg, W. H. E. Schwarz, G. A. Bowmaker, and P. D. W. Boyd, *J. Chem. Phys.*, 1989, **91**, 1762.
77. G. Kresse and D. Joubert, *Phys. Rev. B*, 1999, **59**, 1758–1775.
78. P. E. Blöchl, *Phys. Rev. B*, 1994, **50**, 17953–17979.
79. J. P. Perdew, K. Burke, and M. Ernzerhof, *Phys. Rev. Lett.*, 1997, **78**, 1396–1396.
80. G. Kresse and J. Furthmüller, *Phys. Rev. B*, 1996, **54**, 11169.
81. K. C. Lau, M. Deshpande, R. Pati, and R. Pandey, *Int. J. Quantum Chem.*, 2005, **103**, 866–874.
82. S. Chacko, D. Kanhere, and I. Boustani, *Phys. Rev. B*, 2003, **68**, 035414.
83. F.-Y. Tian and Y.-X. Wang, *J. Chem. Phys.*, 2008, **129**, 024903.
84. A. Heuer, *J. Phys.: Condens. Matter*, 2008, **20**, 373101.
85. G. Daldoss, O. Pilla, G. Viliiani, C. Brangian, and G. Ruocco, *Phys. Rev. B*, 1999, **60**, 3200–3205.
86. C. Peng and H. Bernhard Schlegel, *Isr. J. Chem.*, 1993, **33**, 449–454.
87. R. Hoffmann, P. V. R. Schleyer, and H. F. Schaefer III, *Angew. Chem. Int. Ed.*, 2008, **47**, 7164–7167.
88. J.-I. Aihara, *Theor. Chem. Acc.*, 1999, **102**, 134–138.
89. T. J. KEALY and P. L. PAUSON, *Nature*, 1951, **168**, 1039–1040.
90. Patnaik, P. Handbook of Inorganic Chemicals. 2003..

91. R. G. Parr and R. G. Pearson, *J. Am. Chem. Soc.*, 1983, **105**, 7512–7516.
92. R. G. Pearson, *J. Chem. Sci.*, 2005, **117**, 369–377.
93. J. Zhao, M. Feng, J. Yang and H. Petek. *ACS Nano*, 2009, **3**, 853-864.